Proceedings of ES2008
Energy Sustainability 2008
August 10-14, 2008, Jacksonville, Florida, USA

ES2008-54124

Performance of a Small Network of Grid Interactive, Residential Solar Photovoltaic Systems

Joseph M. Prusa
Teraflux Corporation
Boca Raton, FL, USA

John D. Morris
Florida Atlantic University
Boca Raton, FL, USA

John D. Morris II
No Affiliation
Boca Raton, FL, USA

ABSTRACT

The performance of a network of five recently installed, grid interactive residential solar photovoltaic (PV) systems in Palm Beach County, FL is analyzed, and a probabilistic model for estimating the performance the network is developed. To first order, integrated network performance – whatever the combination of individual PV arrays – can be estimated using generalized tilt factors. These take into account basic geometrical information such as array size/orientation and solar position; as well as atmospheric effects, and module efficiencies. They are computed using a model termed the solar simulator that integrates the instantaneous solar irradiation striking a given PV system over a day. The resulting estimates for mean network performance are within ~ 6% of the observed values. At present, work on estimators of higher moments of the energy production distribution is incomplete, but local meteorological factors that may influence their values as well as data (Pearson correlations and distribution skewness) useful for future developments are discussed.

NOMENCLATURE

k_{tot} total extinction coefficient of one atmospheric mass
k_o average extinction coefficient due to yearly mean conditions
k_v extinction coefficient due to water vapor variations
k_d extinction coefficient due to non vapor aerosol variations
p_{atm} atmospheric pressure (kPa)

ABL atmospheric boundary layer
AO Atlantic Ocean
APS average percent sunshine
CSI clear sky index, a measure of solar energy reaching the ground
DPE_{obs} observed daily production of energy (KWh•day^{-1})
$<DPE>_{bin}$ observed bin averaged daily production of energy
$<DPE>_{mon}$ observed monthly averaged daily production of energy
DPE_{SS} simulated daily production of energy (KWh•day^{-1})
I solar irradiation (W•m^{-2})
I_o solar irradiation at the top of the atmosphere, 1370 W•m^{-2}
M atmospheric mass, value unity at zenith when at STP
MXPWR maximum power output (W) of array on a given day
P probability
PB Palm Beach
RH atmospheric relative humidity (%)
SB sea breeze
SD standard deviation
SS solar simulator (computational model)
T_{atm} atmospheric temperature (^{o}C and ^{o}F)
TF tilt factor

τ_{tot} transparency of the atmosphere

INTRODUCTION

This study focuses on the use of solar photovoltaics (PV) for the generation of grid electrical power. Two commonly cited obstacles to solar PV are (i) it's high cost, especially compared to fossil fuels [1], and (ii) the intermittent nature of solar PV. While a detailed economic analysis is beyond the scope of this study, the historical cost of solar PV has dropped by two orders of magnitude while that of utility generated electricity has risen by a factor of four [2] in the previous four decades. A simple extrapolation of these trends suggests solar PV will become fully competitive with conventional generators within 5 to 10 years.

Here the intermittent nature of solar PV is examined for a small network of distributed, grid tied PV systems. Distributed networks contrast with solar PV "farms" which do not suffer from the grid control issues of distributed networks (Conti and Raiti [3]). Farms also offer economy of scale. Distributed networks, however, allow the use of millions of rooftops, parking lots, and fields for the production of energy. Their distributed nature also enhances network reliability against local inclement weather and local reliability against large scale

grid failure. Finally, solar PV produces peak power at nearly the times when it is most needed, thus offering the possibility of reducing or eliminating the need for conventional peak power generators.

In the following sections, observational and analytical methods are used to develop and benchmark a probabilistic model to predict the performance of a distributed network of PV systems. Ultimate goals for the model are to (i) predict the average expected power, and (ii) estimate the higher moments of the power distribution of a distributed network of PV systems. Data and analyses to date have allowed sufficient model development that the expected power can be estimated with reasonable accuracy, but is not yet sufficient for the higher moments of the probability distributions. "METEOROLOGICAL EFFECTS" gives a quick summary of important local climatic effects that may influence diurnal/weekly variations and induce performance differences due to orientation of PV systems. "DATA" summarizes the data of the systems making up the network followed by in-depth statistical analyses. The data that have been collected includes the daily production of energy (DPE_{obs}), which refers to the collected energy as measured by system charge controllers. This metric is a good indicator of available solar energy, but does not account for inverter and other system losses. In addition to establishing mean levels of performance, it is shown that cloud effects require significant oversizing of the power electronics. Also of note are distribution skewness effects and correlations that clearly reveal distinct differences between some systems, and suggest trends that are indicative of diurnal meteorological effects. "SOLAR IRRADIATION" presents the development of a solar simulator computational model. The solar simulator computes the energy collected by using a combination of first principles, meteorological and atmospheric data, and/or PV system performance data. The simulator is calibrated to the local climate of the network, in effect a mean atmospheric state representative of a time interval of interest. "NETWORK PERFORMANCE" employs the results of the preceding sections to develop a model to predict the mean performance of the distributed network and compares that against observation.

METEOROLOGICAL EFFECTS

Other than the basic diurnal solar cycle, meteorological effects are the most important sources of intermittency. The irradiation incident upon a PV system depends upon (i) local relative humidity and temperature – due to water vapor extinction, as well as (ii) clouds. Additional effects are (iii) wind, which acts to cool PV arrays and thus increase efficiency, and (iv) turbidity which increases atmospheric opacity. The simplest meteorological effect on these variables is seasonal and is easily accounted for in any successful model via the incorporation of mean monthly data.

Much more difficult to predict are intermittent effects with time scales of a few days to weeks. These effects are primarily caused by mid-latitude instabilities known as baroclinic eddies that result in the more familiar jet streams, fronts, and storms (Peixoto and Oort [4]). Many other types of atmospheric time scales greater than one day are known to exist. Prediction of these effects requires sophisticated, state-of-the-art physics and numerical modeling, as well as access to massively parallel processor resources [5-7]; and is beyond the scope of this study. The approach advocated here is to predict mean network power and its weekly to monthly variance in order to establish confidence intervals for expected network power using prior weekly to monthly averaged meteorological and/or PV system power data.

Significant diurnal meteorological phenomena also impact atmospheric variables (i)–(iv). Ubiquitous is atmospheric boundary layer (*ABL*) development. Growth of the *ABL* is due to solar heating of the Earth's surface. *ABL* growth acts to increase atmospheric turbidity due to upward turbulent mixing of low level dust and aerosols – increasing the optical depth of the atmosphere [8-10]. Thus east facing arrays will outperform west facing arrays, other considerations being equal because the atmosphere is more transparent in the morning. *ABL* development also markedly affects cloud cover [10,11]. Unlike the large atmospheric instabilities mentioned previously, diurnal intermittency introduces anisotropy into networks of PV systems with multiple orientations. Other important diurnal effects depend upon local conditions. Examples are sea breezes [11-13], and orographic forcing [14]. Similar to *ABL* development, anisotropic cloud cover from either of these effects may result in differences in west facing arrays vs. other orientations. In the proposed model, diurnal effects will appear in the estimators of the higher moments of the energy production distribution.

The Palm Beach (*PB*) area is a coastal region bounded by the Atlantic Ocean (*AO*) on the east. The ocean produces significant sea breeze (*SB*) effects on the local climate. Inland penetration of *SB* upwards of 30 km [12] can markedly affect temperature and rainfall. Sea breeze fronts are often associated with a linear zone of enhanced cumulus while the shoreward region behind the front is cleared of low level cumulus. Sea breezes are the dominant factor influencing local thunderstorm development in the summer [13]. Regions in the *PB* area within ~5-10 km of *AO* have an average wind of ~ 5 $m \bullet s^{-1}$ (10 mph) throughout the year, whereas 30 km from *AO*, winds only 20% as strong are typical. Lake Okeechobee bounds the northwest *PB* area, and is large enough to induce local climate effects [11] similar to, though weaker than *SB*. Most often, lake breezes result in clearing of low level cumulus clouds up to ~ 8 km uniformly inland from the lake shore, and downwind for ~ 30 km. The diurnal effects associated with sea and lake breezes induce inhomogeneity and anisotropy into network performance because local meteorological conditions differ markedly based upon distance from the ocean or lake.

DATA

PV SYSTEM DESCRIPTIONS

Table 1 lists the basic characteristics of the five systems. Note that system B consists of two sub-arrays, pointing south and west. Table 1 also summarizes the available data records of the five grid tied PV systems that constitute the network of this study. In all but system P1, the record has been contiguous since the start of the data record.

GENERAL STATISTICS OF SYSTEM P2

System P2 provides the longest contiguous record and is used to establish the monthly and seasonal distribution of incident solar radiation. Figure 1 gives an overview of its monthly statistics by showing averages, maxima, and minima for the DPE_{obs}. The yearly average equals 11.3 ± 3.7 $kWh \bullet day^{-1}$, the daily maxima and minima are 18.8 and 0.8 $kWh \bullet day^{-1}$, respectively. With an interval of ~ 30 $days \bullet month^{-1}$, the monthly averages should have a standard deviation (*SD*) of ~ 3.7/ √30 ~ 0.7 $kWh \bullet day^{-1}$. Instead the *SD* of the monthly averages about the yearly mean is ±1.5 $kWh \bullet day^{-1}$. This implies significant seasonal effects in the *PB* area. Assuming a mean PV module efficiency of 13.8% and the array area listed in Table 1, $< DPE >_{yr}$ corresponds to 4.4 $kWh \bullet day^{-1} \bullet m^{-2}$. This is about 15% lower than the standard insolation rate given for Miami, Florida (~ 60 km south of system P2), which is 5.2 $kWh \bullet day^{-1} \bullet m^{-2}$ [15,16].

Figure 2 shows probability density functions (PDF's). They were computed by binning the data into 2.0 $kWh \bullet day^{-1}$ intervals with centerpoints [1.0, 3.0, …17.0]. The PDF's shown correspond to different interval averaging lengths applied to the raw data prior to computing the PDF. For the daily (unaveraged) PDF, a Gaussian 1-2-1 smoothing operator was applied to bins [3.0, 5.0,…15.0]. The solid black line

TABLE 1. PV system characteristics. azimuth corresponds to the usual compass points, e.g., 180^0 is south. Area refers to total array area, and pitch is the angle of the array as rise/run.

SYSTEM	SIZE (kW)	EFF[%]	AREA (m^2)	AZIMUTH	PITCH[#]	LAT[&]	LONG[+]	START[@]	LENGTH[@]
B	1.60, 2.80	17.0%	26.0	180^0, 270^0	26.6^0 , 9.5^0	26^0 38.7’	80^0 4.5’	10/19/07	104 days
P1	4.32	12.6%	35.9	180^0	3/12 (14.0^0)	26^0 23.0’	80^0 5.0’	3/1/07	263 days
P2	2.60	14.0%	18.6	180^0	6/12 (26.6^0)	26^0 21.5’	80^0 6.5’	10/21/06	468 days
X	3.15	13.3%	23.8	270^0	5/12 (22.6^0)	26^0 22.8’	80^0 12.0’	10/5/07	119 days
Y	2.60	14.0%	18.6	180^0	2/12 (9.5^0)	27^0 6.9’	80^0 35.0’	9/3/07	150 days

[%]Nominal module efficiency at 25^0 C and 1000 Wm^{-2} irradiation level.
[#]In parentheses are degrees from the horizontal, with the exception of system B which gives only degrees.
[&]Rounded off to nearest 0.1 minute of arc; [+]Rounded off to nearest 0.5 minute of arc;
[@]START refers to first grid tie day of operation, and LENGTH is length of available record as of January 31, 2007.

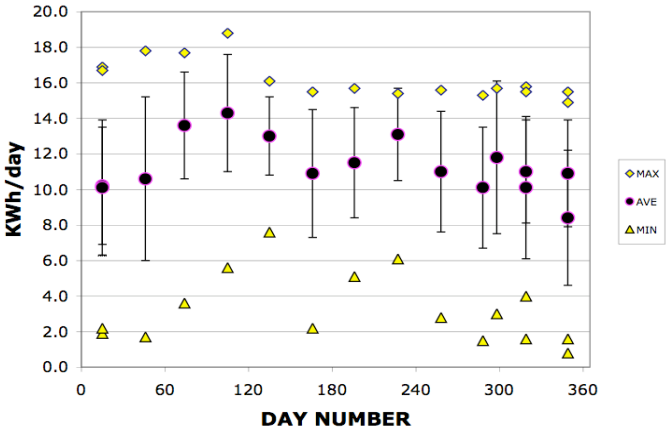

FIGURE 1. Monthly ave, max, min $\langle DPE \rangle_{mon}$ for system P2. Day numbers 1&365 correspond to Jan.1&Dec.31, respectively. Double values for Oct.–Jan., correspond to values from successive years.

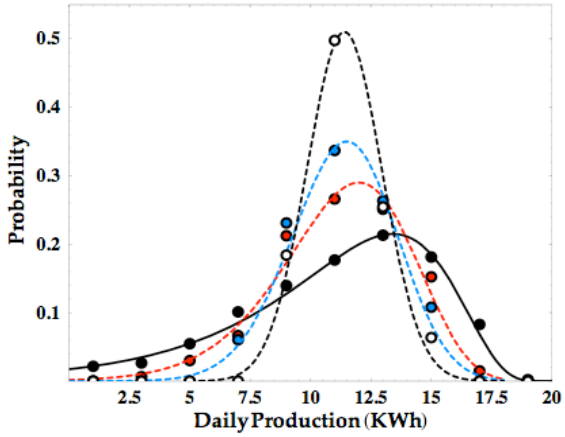

FIGURE 2. Probability density functions for system P2. Functions are shown for data sampled daily (black), and averaged over 3 (red), 7 (blue), and 30 days (black dashed).

depicts this case. The dashed red lines correspond to a 3-day running time average of the data set, the dashed blue line a 7-day running time average, and the dashed black line a 30-day running time average. These PDF’s all have nearly the same average value of ~ 11.3 kWh•day^{-1}, but differ substantially in their *SD*’s and maxima. The unfiltered raw data is skewed negatively, i.e., with a maximum at DPE_{obs} = 13.5 kWh•day^{-1} to the right of the mean, while the 30-day running average is a rough match to a normal distribution with mean = 11.4 kWh•day^{-1} and *SD* = 2.2 kWh•day^{-1}. See summary in Table 2.

TABLE 2. Characteristics of data set for system P2.

AVE. INT.[!]	MEAN	SD	MX	MN	P_{MX}[@]	DPE(P_{MX})[@]
1	11.3[&]	3.7	18.8	0.8	0.21	13.4
3	11.3	2.6	17.5	2.2	0.29	12.0
7	11.3	2.1	15.6	6.5	0.35	11.5
30	11.3	1.5	14.4	8.1	0.51	11.4

[!]AVE. INT. refers to the length of the interval, in days, for the running time average used to filter the data. Value of unity is unfiltered data.
[@]P_{MX} and *DPE*(P_{MX}) refer to the maximum probability and location of the maximum in the PDF’s.
[&]With the exception of column “P_{MAX}”, all value have units of kWh•day^{-1}. For column “P_{MAX}”, the corresponding numbers represent dimensionless probability.

CLOUD REFLECTION/REFRACTION AND THE MXPWR

The design of PV networks requires that the power electronics be sized to the generating capacity of the network. Figure 3 shows an interesting effect whereby the maximum power generated can be substantially greater (35%) than than the nominal power, 2.6 kW, shown in red. It shows daily maximum power (*MXPWR*) as a function of DPE_{obs}. *MXPWR* is the maximum power recorded by the charge controller on any given day. Although the dependency of module efficiency on temperatures can account for significant variations of *MXPWR*, it is not the root cause. Instead refraction of sunlight through thin cirrus, and/or reflection off of the sides of cumulus clouds near the the sun are the primary contributor to this effect. The net effect is that *MXPWR* increases from near zero (very opaque uninterrupted clouds such as stratus) to a maximum in the domain of 5–10 kWh•day^{-1}, followed by a slight decline as the amount of clouds vanish and the *DPE* increases to the maximum value obtained with a very clear sky.

The very clearest days (devoid of clouds or very nearly so) in the dataset are shown by the 25 black data points well below the average *MXPWR* line and on the extreme right in Fig. 3. The DPE_{obs} domain of this subset is (14.6, 18.8) kWh•day^{-1}. The criteria for these points was established, in part, using results from system P1 that provide minute by minute solar irradiation data – and readily show the presence of even slight amounts of clouds. The leftmost, lower points correspond to (i) summer conditions with higher absorption due to water vapor and lower module efficiency due to higher temperatures, or (ii) less solar irradiation in the fall and early winter. The rightmost of these points correspond to cool, late winter or early spring days. These conditions enhance both module efficiency and solar irradiation. This clearest day subset is employed in subsection “CALIBRATION OF EXTINCTION COEFFICIENTS” to calibrate the solar simulator.

In order to attach confidence intervals to the data, it was binned into one unit kWh•day^{-1} intervals except for the end intervals. Due to

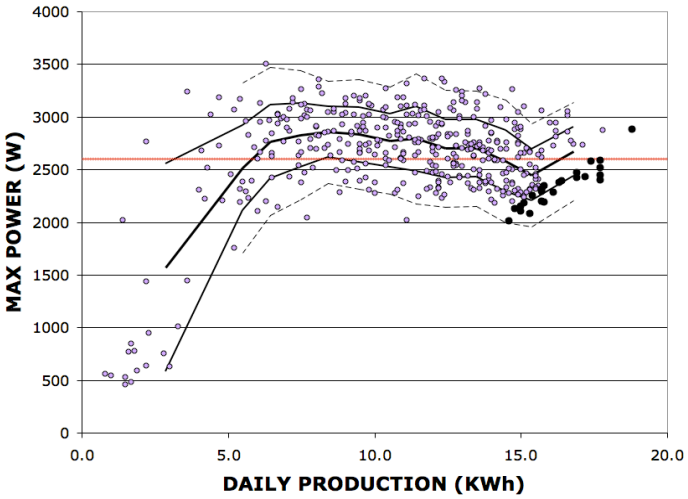

FIGURE 3. Daily maximum power of system P2. The bold line is the average value of an ensemble of points binned in daily production. The lighter and dashed lines correspond to ± 1 and 2 standard deviation units from the mean, respectively. The points set out in bold black along the lower, rightmost border of the dataset denote the 25 clearest days. System P2 is rated at 2.60 kW, shown in red.

scarcity of data at extreme DPE_{obs} (< 5 and > 16 kWh•day^{-1}), the interval for the lowest bin extended from 1.0 to 5.0 kWh•day^{-1}, and the highest from 16.0 to 18.0 kWh•day^{-1}. In each interval the average *MXPWR* and it's *SD* was computed. The mean *MXPWR* is shown as the bold black line in Fig. 3, it begins and ends at the interval midpoints of the first and last bins. The light solid lines show the mean ± 1.0 *SD*, while the black dashed lines show the average value ± 2.0 *SD*. Assuming a normal distribution for the data, these inner and outer bands denote 68% and 95% confidence intervals, respectively. In fact, the outer band captures 97% of the data. Averaged over all bins, 18% of the *MXPWR* data lie at ≥ 3.0 kW; 4.5% and 0.9% levels occur at 3.2 and 3.35 kW, respectively. These three values of *MXPWR* are 15%, 23%, and 29% greater than the 2.60 kW design value.

STATISTICS OF THE INDIVIDUAL SYSTEMS

Statistics averaged over long enough intervals – roughly one month as evidenced in Fig. 2 – should be roughly comparable since the underlying distributions will be normal. There is no such assurance for the daily statistics. This is important when making probabilistic load flow calculations of the effect of distributed networks on the grid [3]. The non-normalcy of distributions is readily shown by skewness. In a skewed distribution, the variable spends most of its time at either higher (negative skewness) or lower (positive skewness) values than the mean.

Table 3 lists the skewness of the distributions for DPE_{obs}, for the five network systems, for 75 days of common observations in the period November 1, 2007 to January 30, 2008. The record is not contiguous because one of the systems has a discontinuous record during this interval, with missing data on November 20 and December 16-31, 2007. Figure 4 shows the distributions for systems B, X, and Y, making the skewnesses visually evident. (Fig. 2 shows the full data set of P2, and has a skewness of -0.61). The mean skewness of the five systems and the *SD* of the skewness are -0.18 and 0.65, respectively. Only the skewness for system Y lies outside of a 90% confidence interval for zero. It is also distinctly positive compared to the other four PV systems, and satisfies Chauvenet's criterion for an outlier. Table 4 gives the Pearson correlations and distances between systems.

TABLE 3. Summary statistics of the five PV systems.

SYSTEM	B	P1	P2	X	Y
$<DPE>_{obs}$ [@]	14.8	14.9	10.6	8.7	3.9
SD[@]	4.0	4.2	3.2	2.3	0.8
Skewness	-0.73	-0.46	-0.48	-0.16	0.93
SD/$<DPE>_{obs}$	0.27	0.28	0.30	0.26	0.20
$<DPE>_{obs}$/SIZE	3.35	3.45	4.08	2.76	1.49

[@]Units of kWh•day^{-1}

TABLE 4. Correlation–Distance (km) Matrix. All correlations are significant at the 0.01 level (2-tailed) except for system Y.

SYSTEM	B	P1	P2	X	Y	AO[%]
B	*	0.806 (29.0)	0.804 (31.9)	0.739 (31.8)	0.064 (72.2)	(3.9)
P1	0.806 (29.0)	*	0.937 (3.4)	0.807 (11.4)	0.041 (94.7)	(2.0)
P2	0.804 (31.9)	0.937 (3.4)	*	0.762 (9.8)	-.066 (96.1)	(3.7)
X	0.739 (31.8)	0.807 (11.4)	0.762 (9.8)	*	0.146 (89.6)	(13.4)
Y	0.064 (72.2)	0.041 (94.7)	-.066 (96.1)	0.146 (89.6)	*	(41.2)

[%]Atlantic Ocean

The correlations and inspection of bivariate scatter plots indicate significant linearity between all systems except for system Y, which is uncorrelated with the other four systems.

Severe shading of system Y occurred near the winter solstice, and this greatly reduced DPE_{obs} as well as attenuated the variance of that data set (diffuse radiation is much smoother than direct radiation). The net result is similar to the effect of clouds, which increase skewness. Negative skewness, by contrast, corresponds to mostly clear skies – where the system spends more of its time at higher energy production rates than the mean. In the *PB* area, this is the more representative case, and it is indicative of systems B, P1, and P2. The skewness for system P2 fits a linear relation with $< DPE >_{mon}$ with $r^2 = 0.44$.

System Y is also least affected by sea breeze (*SB*) flows. Table 4 gives the distances of systems from the Atlantic Ocean (*AO*). It can be seen that systems B, P1, and P2 are close to the Atlantic Ocean and well within *SB* flow regimes. System X is close enough to typically experience a *SB* flow, but one to several hours later in the day compared to the first three systems. System Y is sufficiently far from the ocean to not experience sea breeze effect much of the time [12,13] – but at only 8.6 km, it is close enough for possible Lake Okeechobee lake breeze effects [11]. The effect on any normalized random variable *Z* affected by *SB* is that the values of *Z* would be similar in systems B, P1, and P2; that *Z* would be most dissimilar for system Y (furthest from *AO*), and that *Z* would be intermediate in value for system X. In addition to skewness, Table 3 lists two other candidate variables for discerning *SB* effects: a dimensionless standard deviation $SD/<DPE>_{ob}$, and $<DPE>_{obs}$/SIZE which is a dimensionless mean production rate.

Systems B, P1, and P2, which have the strongest (and almost identical) sea breeze flow regimes, are the most highly correlated with each other with a mean correlation of 0.85 (computed from the mean r^2). The mean of the correlations of these three systems with X, which is in a reduced sea breeze flow regime is 0.77. Finally, the correlations of all systems with Y, which has at most, only minor sea breeze effect, is not significantly different from zero (the correlation of Y with X of 0.15 is the largest of the four).

Another possible diurnal effect is that the somewhat degraded

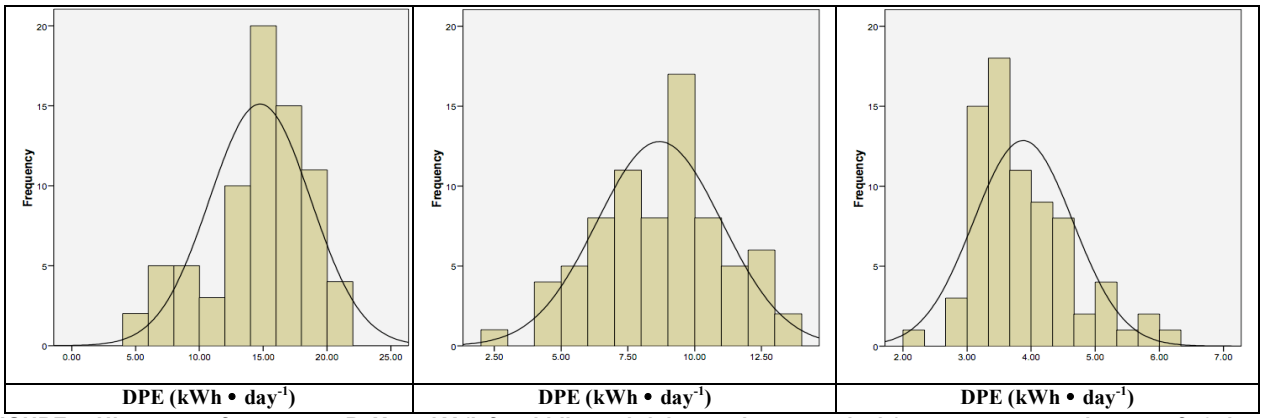

FIGURE 4. Histograms for systems B, X, and Y (left, middle, and right panels, respectively), over a common data set of 73 days.

performance of system X (west facing) compared to B, P1 and P2 may be due to increased atmospheric turbidity – the *ABL* effect alluded to earlier. One more possibility is that the distance between system Y and the others (> 72 kms) is simply greater than the integral scale at which daily signals become uncorrelated [17], even if the turbulence underlying the atmospheric flow is homogeneous. From this viewpoint, the data given in Table 4 could represent autocorrelations of an underlying distribution at select distances; whereby sea breeze flows introduce anisotropy. At present, the data are suggestive, but do not discern any particular mechanism.

SOLAR IRRADIATION

Given that the statistics of the higher moments are not definitive, it is of great interest to know if it is possible to reasonably predict network performance based upon *mean* observations. Furthermore, it is of interest to make the prediction based upon the performance of *one* system, such as P2. The quality of this result depends upon:

(i) DPE_{ob} data collected at P2 can be normalized in such a way so as to give the the energy generation (or solar irradiation levels) for arbitrary array size and orientation.

(ii) The effects of local weather (clouds, atmospheric transparency, etc.) at each PV system location can be estimated.

In addition to local climate considerations, a key ingredient is the development of an algorithm termed the "solar simulator" (*SS*), which computes the instantaneous power produced by a PV array. Integration over the course of a day yields energy production. If the array size and orientation are matched to those of system P2, comparison of clear sky energy production with the observed data allows the model to be calibrated such that a model appropriate for the *PB* area is available. Thus *SS* can be used to predict the performance of any other PV system in the network. The caveat is that the statistics be the same throughout the *PB* area. Although this is not rigorously true on an hour by hour basis (*SB* effects, passages of fronts through the region, etc.), the available data suggests it may be a reasonable, albeit crude approximation for the averaged statistics of the previous section.

THE SOLAR SIMULATOR

Computation of the local position of the sun is a standard exercise in celestial mechanics. References [18–20] are sufficient, with the last being especially useful as a "hands on" manual. The current state of the art in computing the position of the sun allows one to do so with sub arc second accuracy – far beyond the needs of solar irradiation estimates. By contrast, computation of the properties of the atmosphere is much more of an "art". The level of sophistication to accurately predict atmospheric properties, even statistics, is many orders of magnitude more difficult than solar position computations. As a result, this study employed a reductionist approach on the atmospheric property side – and computed the instantaneous clear sky irradiation falling on the orientated array surface using well understood bulk atmospheric properties. The current algorithm is based upon the following:

1. *Orbit of the Sun:* A "low accuracy" approach [20] is employed, yielding a solar positional accuracy of ~ 30 seconds of arc (a higher accuracy example is given in [22]). Consistent with this level of accuracy, higher order effects of (i) perturbations from the other planets, (ii) deviation of the geoid (shape of the Earth), (iii) nutation of the Earth's axis, and (iv) the aberration of light are not considered. The model does incorporate (v) epoch dependent eccentricity of the Earth's orbit (the default year is 2010.0), (vi) a correction for light travel time (from the sun to the Earth), and (vii) correction for precession of the equinoxes (again set to year 2010.0 as default).

2. *Properties of the Atmosphere*: A locally "lumped atmosphere" approach is utilized. The model does not attempt (i) to employ detailed wavelength dependent, multidimensional radiation transmission functions, nor (ii) to distinguish diffuse from direct beam radiation [23]. It also does not include (iii) inhomogeneous atmospheric properties beyond the mean vertically stratified structure, nor (iv) magnification at the horizon. The *SS* model does incorporate empirical expressions for atmospheric (v) mass modified to allow for atmospheric pressure (p_{atm}) variations following Rosenberg [24] ;

$$M = \left(\frac{p_{atm}}{101.3\,kPa}\right)\left\{\cos(Z) + \exp\left[-11 + \left(\frac{\cos(Z)}{40}\right)\right]\right\}^{-1} \qquad (1)$$

where Z is the zenith angle, and (vi) refraction (R_f), after Meeus [20];

$$R_f = 1.02\left(\frac{p_{atm}}{101.3\,kPa}\right)\left(\frac{283K}{273K + T_{atm}}\right)\left\{\tan\left[M + \left(\frac{10.3}{M + 5.11}\right)\right]\right\}^{-1} \qquad (2)$$

that allows for bulk pressure and temperature (T_{atm}) effects. *SS* employs (vii) a Bouguer-Lambert extinction law for atmospheric transparency [24]:

$$\tau_{tot} = I / I_o = \exp(-k_{tot}\,M) \qquad (3)$$

$$k_{tot}\,M = (k_o + k_v + k_d)\,M = -\ln(\tau_{tot}) \qquad (4)$$

and the mean vertical stratification of the atmosphere is accommodated using the atmospheric masses along the light path. Here τ_{tot} is the total atmospheric transparency, and $k_{tot}M$ the corresponding optical depth. The solar irradiation is denoted by I, and I_o = 1370 W•m^{-2} is its

magnitude at the top of the atmosphere. To first order, M is influenced by pressure (~ atmospheric weight), but not temperature. The various extinction coefficients account for the absorption of a standard airmass (k_o), water vapor variations (k_v), and variations due to other aerosols and dust (k_d). For the standard airmass, k_v and k_d are specified constants that are absorbed into the definition of k_o, that is, the extinction is set solely by k_o, which is determined inversely from the observed data for clear days in the following section. The effects of variable water vapor are modeled in *SS* using the Clausius-Clapeyron equation, given the relative humidity *RH* and temperature T_{atm}. *SS* can also take into account variations of non vapor aerosol extinction, if data for such effects are available. See the following subsection for details. Pressure, temperature, and relative humidity data can reasonably be input as monthly averages or for higher accuracy, when such data are available, distributed daily or even diurnally [24].

3. *Properties of the PV arrays modeled*: Required information for each PV system are (i) size, (ii) module efficiency vs. temperature, (iii) location (latitude, longitude, altitude), (iv) orientation (pitch, azimuth), (v) date(s), and (vi) temperature and pressure data corresponding to the time interval of interest. The temperature and pressure data are also employed in the atmospheric mass computation. An option is to employ two temperatures, one for atmospheric properties, and a second higher temperature for module temperature, in accord with (a) steady state energy balance considerations (e.g., conduction, convection, and/or radiation heat transfer analyses [27]) or equivalently, (b) in terms of the nominal operating cell temperature (NOCT [16]). An approximately linear response of the form $T_{mod} = T_{atm} + c\,I$ results.

4. *Organization of the computation*: Once all required input are given, the algorithm computes the distance to the sun, the resulting irradiation at the top of the atmosphere, the solar coordinates as seen from the PV array location (including refraction and light travel time), the resulting angular distance from the sun to the orientation point of the array (defined as the point on the celestial sphere perpendicular to the PV array surface), the atmospheric mass, and ultimately the instantaneous incident irradiation striking the array. These values are integrated over the duration of a day to compute the total solar irradiation under clear sky conditions. An integration timestep of 0.5 h gives evaluations of DPE_{SS} converged to three significant figures. Elements of precession and eccentricity vary slowly and do not need to be updated even over several years of integrations.

CALIBRATION OF EXTINCTION COEFFICIENTS

The extinction coefficients k_o, k_v, and k_d in Eq. (4) are determined from the dataset for system P2. An essential prerequisite for the data to be used are that they be as free as possible of (i) clouds and (ii) aerosols other than water vapor, such as smoke, dust, and pollutants. In practice, condition (i) is well met if $DPE_{obs} > 14.5$ KWh•day^{-1} and *MXPWR* lies ~ one or more standard deviations units below the mean *MXPWR* line in Fig. 4. See the discussion in subsection "CLOUD REFLECTION/REFRACTION AND THE MXPWR" for additional details. Termed *clearest days*, none were observed for December 2006-07 or August 2007. For the extinction coefficient analysis, these 25 points were binned according to month, and in each bin the data were averaged for daily observed values of DPE_{obs}, *RH* and T_{atm} [24], and day of the year. These last three conditions were input to *SS*, and the total extinction coefficient k_{tot} was adjusted until *SS* computed a value of *DPE* that matched the observation. The results are presented in terms of the total transparency, τ_{tot}, shown in Fig. 5, and are also summarized in Table 5.

The average total transparency $<\tau_{tot}>$, equal to 75.1%, of the 10 points listed in Table 6 defines the yearly mean extinction coefficient

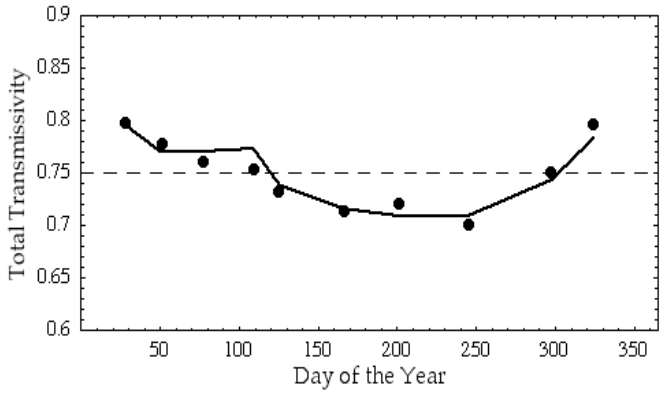

FIGURE 5. Water vapor aerosol extinction. The average transparency of 75.1% is depicted by the horizontal dashed black line. The bold line shows the water vapor correction, explained in the text.

per unit airmass, $k_o = -\ln(<\tau_{tot}>) = 0.287$. From Eq. (1), this leads to an expression of familiar type [16]:

$$I/I_o = (0.75)^M \tag{5}$$

where it is understood that the average transparency accounts for a mean aerosol extinction effect in addition to other effects like Rayleigh scattering and ozone absorption [26].

Spatially inhomogeneous aerosols strongly influence optical depth on scales ranging from minutes to years. Although variations in water vapor and dust are generally the most significant sources of variability in extinction coefficients, in the *PB* area water vapor is the dominant variable aerosol factor. In this study, daily and seasonal variations of water vapor extinction are accounted for, and it is assumed, barring data to the contrary, that $k_d \sim 0$. Much less common, extreme variations in optical depth can also occur from wildfire smoke. *SS* can accommodate such effects, but data are required to estimate either the optical depth of the atmosphere, or the value of k_d – see the example at the end of this subsection. Regards k_v, the key idea is that given the value of k_o, a correction function for k_v is constructed using the Clausius-Clapeyron eq. [27] as follows:

$$k_v = A\left[p_v(T_{atm}) \bullet RH - B\right] \tag{6}$$

$$p_v(T_{atm}) = p_{vr} \exp\left[\frac{h_{fg}}{R}\left(\frac{1}{T_r} - \frac{1}{T_{atm}}\right)\right] \tag{7}$$

where p_v is the vapor pressure, $(h_{fg}/R) = 5314$K, and $p_{vr} = 2.487$ kPa at $T_r = 294.1$ K. T_{atm} and *RH* are input parameters given in Table 5. The constants A and B are chosen so that the resulting function $k_o + k_v$ gives a least squares best fit to the observed total extinction. Figure 5 shows the best fit $A = 0.052$ and $B = -1.77$ in terms of total transparency. This expression for vapor aerosol extinction predicts that extremes in water vapor pressure during the year, say from ~ 0.62 kPa (late winter) to ~ 3.6 kPa (August) will generate changes of $\Delta k_v \sim 0.19$, in general agreement with the value of ~ 0.2 given in [26] for the differences between very dry and humid nights at sea level.

Aerosol optical depth data may also be input directly into *SS*. Such data are now routinely available via GOES satellite remote sensing [28]. An example of special interest occurred on May 13, 2007, when smoke from wildfires covered much of Florida. GOES imagery at ~ 10am local time on this day indicated aerosol optical depths of $k_{tot}M \sim 0.6$ to 1.2 over S. Florida, with higher values directly over the *PB* area, where visibility was recorded as ~ 8 km (5 miles).

TABLE 5. Characteristics of clearest sky data subset of system P2.

BIN	**1**	**2**	**3**	**4**	**5**	**6**	**7**	**8**	**9**	**10**
DAY NO.	28	51	77	109	125	166	201	245	297	324
DATE	Jan 28	Feb 20	Mar 17	Apr 18	May 4	Jun 14	Jul 19	Sep 1	Oct 23	Nov 19
NO. PTS.	2	4	2	4	3	3	3	1	2	1
$< T_{atm} >^{\&}$	63.5°F	71.0	70.0	76.5	84.5	87.0	88.0	91.0	80.0	70.0
$< RH >^{\&}$	33.0%	49.0	51.0	38.5	51.5	61.0	63.0	58.0	56.0	39.0
$< DPE >_{bin}^{\#}$	16.6	17.0	17.7	17.5	15.9	15.0	15.3	15.1	15.4	15.8
τ_{tot}	.798	.777	.761	.754	.732	.714	.721	.701	.751	.796

$^{\&}$Values are rounded off to the nearest 0.5 unit; $^{\#}<DPE>_{bin}$ is observed bin averaged value, in KWh•day^{-1}.

At this time, the clearest airmass lay offshore to the south. Winds generally from the south improved visibility to 14.5 km (9 miles) from noon to ~3pm, at which point visibility decreased to 6.4 km (4 miles) by ~ 5pm and then to 4.8 km (3 miles) an hour later. These data may be compared with computations using *SS* and the observed data for array P2. Optical depth values may be inferred by employing *SS* to solve the problem inversely, either on average utilizing the observed DPE_{obs} = 11.1 KWh•day^{-1}, or for the minimum value by utilizing the observed *MXPWR* = 2023W, assumed to have occurred near solar noon (and assuming no cloud effects as discussed in "CLOUD REFLECTION/ REFRACTION AND THE MXPWR"). The resulting values (given T_{atm} = 28.0°C (83°F) and *RH* = 49%; from [24]) are $k_{tot}M$ = 0.61 (average) and 0.43 (minimum). The "nominal" optical depth is 0.30 on this date for the given (T_{atm}, *RH*).

COMPARISONS WITH SEASONAL DATA

With calibrated extinction coefficients, it is possible to utilize *SS* to make predictions about the overall solar energy capture during the year, provided one can estimate the energy loss due to clouds. If performance data are not already in hand, this can be done through use of the average percent sunshine (*APS*), determined as a part of the national climate record. A *clear sky index* (*CSI*) is defined to be the ratio of observed $<DPE>_{mon}$ to simulated clear sky DPE_{SS} predicted by *SS* using monthly averaged properties shown in Table 6, according to:

$$< DPE >_{mon} = CSI \bullet DPE_{SS} \qquad (8)$$

CSI is solved for inversely, given the known performance $<DPE>_{mon}$ and the corresponding computational result DPE_{SS}. The *CSI* is then compared directly against monthly values of *APS*, averaged over 17 years through 1993 for Miami, FL (approximately 60 km south), for which data are available (NCDC [29]). Table 6 summarizes the monthly averaged temperatures and relative humidities of the atmosphere (also from [29]) as well as the *CSI* results (the simulations did not employ temperatures or relative humidities that varied during the day but instead employed mean values representative of the times of significant solar output).

Analysis of the *CSI* – *APS* difference indicates a mean deviation of 1.2% with *SD* = 4.6%. Thus the mean lies well within the 95% confidence interval (-2.7, 2.7) of zero. The deviation of all months are also ≤ 9%, or 2 *SD* units. We conclude that both *CSI* and *APS* (assuming underlying normal distributions) represent the same statistical measure of cloud effects at a 95% level of confidence.

NETWORK PERFORMANCE

GENERALIZED TILT FACTOR

Recall that Table 3 lists summary statistics for all five PV systems during the 75 common days between November 1, 2007 and January 30, 2008. Of special interest here is the ratio $<DPE>_{obs}$/SIZE, which gives a partial normalization of observed system performance. This is the quantity that must be estimated in order to estimate network performance. Since system P2 had the largest value (due to having the best orientation, see Table 1), it is used to further normalize the observed performances, as:

$$TF_{obs} = (SIZE_{P2} \bullet < DPE >_{obs}) / (SIZE \bullet < DPE >_{obs,P2}) \qquad (9)$$

where *TF* is termed a *tilt factor*, named so as to account for the geometrical effects of array orientation and solar trajectory through the sky. These effects are readily estimated with the *SS*, assuming constant atmospheric properties, simply by comparing the same array but with different orientations. The resulting TF_{obs} are listed in Table 7.

Since the solar trajectory changes on a seasonal time scale, seasonal variations in atmospheric transparency also affect normalized performance. *TF0* is defined as a *generalized tilt factor* that incorporates geometrical effects as well as seasonal transparency variations:

$$TF0 = DPE_{SS}(design) / DPE_{SS}(south - ecliptic) \qquad (10)$$

Note that any other parameters that remain constant during a day of integration have no impact, such as the clear sky index (clouds). *TF0* is computed using seasonal atmospheric data (Table 6), on 6 discrete days in the November 1, 2007 – January 30, 2008 interval. The procedure is to compute DPE_{SS} on the specified day, for given design conditions, and then repeat the computation changing only the array orientation to the optimum south–ecliptic pointing. These six values are integrated, avoiding the discontinuous segments, to produce the 75 day average tilt factors $<TF0>$, listed in Table 7. A quick glance reveals that $<TF0>$ models the bulk of the observed variations (e.g., TF_{obs}) except for system Y, which suffers from severe shading. To leading order, the shading effect reduces system Y's output to only (.37/.82) = 44% of it's design value. $<TF0>$ appears to provide a reasonably good match for systems P1 and X, but for system B it is low.

To improve upon $<TF0>$, the effects of module efficiency are added. Modules from different manufacturers generally have different standard efficiencies (at standard conditions of I = 1000 W•m^{-2} and T_{pv} = 25°C these efficiencies are close to the mean values during winter). The manufacturer specified standard efficiencies $<\eta>$ are given in Table 7 with the following modifications: (i) due to comparison with the seasonal data (Table 6), $<\eta>$ for system P2 has been increased from the manufacturer's value of 14.0% (this modified value is well within the +10% maximum power limit specified by the manufacturer), and (ii) $<\eta>$ for system P1 has been increased from the manufacturer's value of 12.6% based upon a simulation using *SS* to model the minute by minute output of system P1 on April 7, 2007, one of the 25 elements of the clearest sky data subset of system P2 represented in Table 5. Assuming uniform $<\eta>$ throughout the day (detail-

TABLE 6. Monthly averaged properties and simulated clear sky index for 2006-08 for system P2.

MONTH	Jan	Feb	Mar	Apr	May	Jun	Jul	Aug	Sep	Oct	Nov	Dec
DAY NO.[@]	15	45	74	105	135	166	196	227	258	288	319	349
$< T_{atm} >^{\&}$	21.0°C	21.0	23.5	23.5	25.5	28.0	29.0	29.0	27.0	27.0	23.0	23.0
$< T_{atm} >^{\&}$	70.0°F	69.5	74.0	74.5	78.0	82.0	84.0	84.0	80.5	80.5	73.5	73.0
$< RH >^{\&}$	62.5%	57.0	50.5	51.5	56.5	63.0	60.5	63.0	69.5	69.5	60.5	66.0
$< DPE >_{mon}^{\#}$	10.2	10.6	13.6	14.3	13.0	10.9	11.5	13.1	11.0	10.5	10.6	9.7
$DPE_{SS}^{\#}$	14.6	16.8	18.1	18.5	17.3	16.1	16.1	16.5	16.6	15.5	14.8	13.4
CSI	70%	63	75	77	75	68	71	79	66	68	72	72
$APS^{\%}$	67%	67	74	76	72	69	73	73	72	71	66	63
CSI-APS	3%	-4	1	1	3	-1	-2	6	-6	-3	6	9

[@]At mid month; [&]Values are rounded off to the nearest 0.5 unit; [#]Units of kWh•day^{-1}; [%]17 year average through 1993.

TABLE 7. Performance estimates for the five PV systems.

SYSTEM	B	P1	P2	X	Y
TF_{obs}	0.823	0.848	1.000	0.676	0.366
$< TF0 >$	0.712	0.878	1.000	0.649	0.824
$<\eta>$	17.0%	13.8	14.8	13.3	14.8
$< TF1 >$	0.818	0.819	1.000	0.608	0.824
Ψ_0	-0.135	0.035	0.000	-0.040	1.25
Ψ_1	-0.006	-0.034	0.000	-0.101	1.25

ed efficiency functions are currently available only for system P2), an efficiency correction is used in defining the generalized tilt factor:

$$< TF1 > = < TF0 > \bullet < \eta > / < \eta >_{P2} \qquad (11)$$

listed in Table 7. $<TF1>$ appears markedly better for system B, but somewhat worse for X (system Y is unchanged because it uses the same modules as P2). In order to assess the predictive skill of these tilt factors, confidence intervals are computed for the normalized variables $\Psi_0 = <TF0> \bullet TF_{obs}^{-1} - 1$ and Ψ_1 (defined similarly but using $<TF1>$). These normalized values are given in the last two rows of Table 7, and if symmetric, should equal zero. The values for system Y appear a distinct outlier. Ψ_0, Ψ_1 do not represent it adequately (primarily due to shading effects). A quick application of Chauvenet's test confirms that these values can be rejected as not representative. The means and SD's for the four remaining systems (B, P1, P2, and X) are -0.035 ± 0.074 and -0.035 ± 0.046 for Ψ_0 and Ψ_1, respectively. Both means are deep within 95% confidence intervals for zero. However since the SD for Ψ_1 is only 63% of that for Ψ_0, $<TF1>$ is the better estimator for determining network performance.

ESTIMATE OF MEAN NETWORK POWER & COMPARISON

The performance of a network of N solar PV systems is now computed as:

$$< DPE >_{net} = \left(\frac{< DPE >_{ref}}{SIZE_{ref}} \right) \sum_{k=1}^{N} < TF1 >_k \bullet SIZE_k \qquad (12)$$

where subscript 'ref' denotes a reference system for which generalized tilt factors $<TF1>$ are computed. In the preceding section, system P2 was used as the reference system, but in practice nearly any choice is a reasonable alternative, e.g., the reference system could be one pointed at the zenith. Also, the reference can be either observed or simulated.

As a first example, Eq. (12) is used to estimate the performance of the network of five PV systems, a priori, utilizing only the observed performance of reference system P2. Thus $<DPE>_{ref} / SIZE_{ref} = 10.6/2.6 = 4.08$ from Table 3. Appropriate values for $<TF1>$ and *SIZE* listed in Tables 7 and 1, respectively, are then entered into Eq. (12) with the result that $<DPE>_{net} = 56.3$ kWh•day^{-1}. This example corresponds to the case where initial performance data for a single PV system is available to estimate power of a network of distributed systems.

As a second example, the computational model *SS* is employed to estimate $<DPE>_{ref}$. This corresponds to the case where no initial data are available, and simulations based upon observed climatology must be used exclusively to estimate the performance of the systems comprising the network. In this case, *SS* is used to simulate $<DPE>_{ref} = <DPE>_{P2,SS} \bullet APS$, following Eq. (8) and Table 6, for the 6 discrete days in the 75 common day interval mentioned previously – note that *APS* is a proxy for *CSI* which is unknown in this case. The resulting values are then integrated as done previously for the tilt factors, resulting in $<DPE>_{ref} = 9.51$ kWh•day^{-1}. Thus $<DPE>_{net} = 50.5$ kWh•day^{-1} (Eq. (12) scales proportionately to the value of $<DPE>_{ref}$).

Actual network performance is shown in Figure 6. The average value is $<DPE>_{net} = 52.8$ kWh•day^{-1} (with a SD = 12.8 kWh•day^{-1} and skewness = -0.56). Thus the first example result is 6.5% high, while the estimate from the second example is 4.5% low, and it appears that the two methods are about equally effective in estimating network performance. Considering the known biases in the data, such as (non-Gaussian) shading effects, and differences between historical climatology and actual conditions, the results are surprisingly good.

As a final point, note from Fig. 6 that the variance appears to generally increase as the data move from November (on the left) to

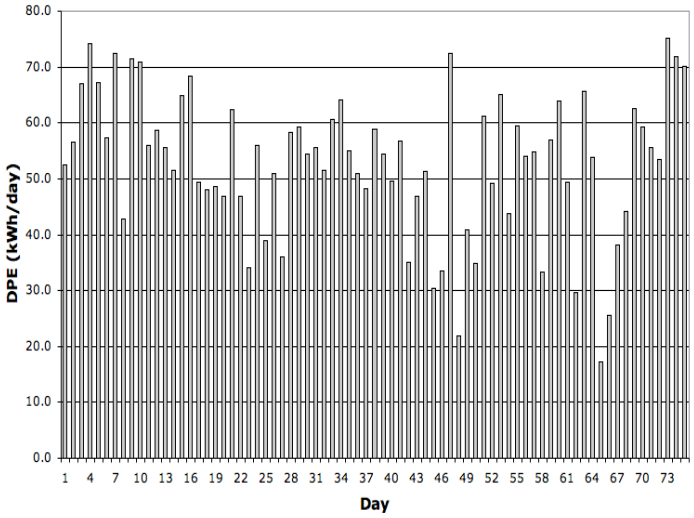

FIGURE 6. Network performance for the 75 common days between November 1, 2007 – January 30, 2008. Missing data are for November 20 and December 16-31, 2007.

January (on the right). Although not computed, other moments may also be showing trends as the weeks pass. Not only do the distributions of systems differ, as shown in "DATA", but apparently distributions for single systems and/or networks also evolve in time.

CONCLUSIONS

A probabilistic model useful for estimating the daily production of electrical power by a network of solar PV systems is outlined in this study. The model is based upon careful statistical analysis of the power production distributions of a prototype network; as well as a solar simulator based upon elementary celestial mechanics, atmospheric optics, meteorology, statistics and engineering principles. Results indicate that when based upon average daily statistics, the model can predict network performance to within engineering accuracy, provided care has been taken to calibrate it for the local climate. Additional points of note follow.

- Cloud focusing effects require power electronics to be oversized ~35% above nominal power
- Shading effects cause positive tendencies in distribution skewness. Cloudiness causes positive tendencies in skewness, while clear skies promote negative tendencies.
- Although not definitive, data for a westward facing array suggests it does not perform as well as simple geometrical considerations would suggest. This is consistent with local climate effects that decrease solar irradiation when western pointing arrays collect the greatest power.
- Regional, daily to monthly fluctuations in water vapor and dust loads have significant impact on atmospheric transparency, and should be incorporated into model predictions of network performance.
- It is anticipated that corrections for non-normal distributions can be estimated from local meteorological conditions and PV array orientation. Higher moment considerations will also allow confidence intervals for the estimated power production to be established.
- The model can be applied to time scales as short as desired – provided that appropriate higher resolution historical system performance or local climate data are available. Model output at shorter than daily scales could be input into a probabilistic load flow model [3] to determine the interaction of the distributed network and grid with respect to slow voltage and current variations at the desired time scale.

ACKNOWLEDGMENTS

The Authors thank R. Brown, J. Prado, W. Xu, and P. Yorke for making performance data from their PV systems available for this study; and the Reviewer that helped clarify the presentation.

REFERENCES

1. Borenstein, S. ,"The Market Value and Cost of Solar Photovoltaic Electricity Production", Working paper WSEM WP 176, Center for the Study of Energy Markets, University of California Energy Institute, Berkeley, CA, 2008.

2. Annual Energy Review (AER), Report DOE/EIA-0384 (2005); http://www.eia.doe.gov/emeu/aer/elect.html

3. Conti, S., and Raiti, S., "Probabilistic Load Flow Using Monte Carlo Techniques for Distribution Networks with Photovoltaic Generators", *Solar Energy*, **81**, 2007, 1473-1481.

4. Peixoto, J.P., and Oort, A.H., Physics of Climate. American Institute of Physics, NY, 1992, 520p.

5. Collins, W.D., et al., "The Formulation and Atmospheric Simulation of the Community Atmosphere Model: CAM3. *J Climate*, **19**, 2006, 2144-2161.

6. Prusa, J.M., Smolarkiewicz, P.K., and Wyszogrodzki, A.A., "EULAG, a Computational Model for Multiscale Flows. *Comp. & Fluids*. doi:10.1016/j.compfluid.2007.12.001 (in press), 2008.

7. Abiodun, B.J., Prusa, J.M., and Gutowski Jr, W.J., "Implementation of a Non-Hydrostatic, Adaptive-Grid Dynamics Core in CAM3. Part I: Comparision of Dynamics Cores in Aqua-Planet Simulations." *Climate Dynamics* (in press), 2008.

8. Eaton, F.D., Hines, J.R., Drexler, J.J., and Soules, D.B., "Short Term Variability of Atmospheric Turbidity and Optical Turbulence in a Desert Environment", *Theor. Appl. Climatol.*, **56**, 1997, 67-81.

9. Pielke, R.A., and Pearce, R.P., eds., Mesoscale Modeling of the Atmosphere. *Meteorological Monographs*, **25**, Chap. 2, 18-19, American Meteorological Society, Boston, 1994, 167 p.

10. Garrett, J.R., The Atmospheric Boundary Layer. Cambridge University Press, 1992, 316 p.

11. Segal, M., Leuthold, M., Arritt, R.W., Anderson, C., and Shen, J., "Small Lake Daytime Breezes: Some Observational and Conceptual Evaluations", *Bull. Amer. Meteor. Soc.*, **78**, 1997, 1135–1147.

12. Arritt, R.W., "Effects of the Large-Scale Flow on Characteristic Features of the Sea Breeze", *J. Appl. Meteor.*, **32**, 1993, 116–125.

13. Cetola, J.D., "A Climatology of the Sea Breeze at Cape Canaveral, FL", MS Thesis, The Florida State University, 1997.

14. Smith, R.B., "The Influence of Mountains on the Atmosphere", *Advances in Geophysics*, **21**, 1979, 87-230.

15. NREL, National Renewable Energy Laboratory, Solar Resource Information, Solar Maps, Golden, CO, 2008. http://rredc.nrel.gov/solar/old_data/nsrdb/redbook/atlas/

16. Messenger, R.A., and Ventre, J., Photovoltaic Systems Engineering, 2nd ed. CRC Press, Boca Raton, FL, 2004, 455p.

17. Tennekes, H., and Lumley, J.L., A First Course in Turbulence. MIT Press, 1980, 300p.

18. Taff, L.G., Celestial Mechanics. John Wiley & Sons, New York, 1985, 520p.

19. Meeus, J., Astronomical Algorithms. William-Bell, Richmond, VA, 1991, 429p.

20. Duffett-Smith, P., Practical Astronomy with Your Calculator, 3rd ed. Cambridge University Press, 1988, 185 p.

21. Reda, I., and Andreas, A., "Solar Position Algorithm for Solar Radiation Applications", *Solar Energy*, **76**, 2004, 577-589.

22. Bird, R.E., and Hulstrom, R.L., "A simplified clear sky model for direct and diffuse insolation on horizontal surfaces", Solar Energy Research Institute, SERI/TR-642-761, Golden, CO, 1981.

23. Rosenberg, G.V., Twilight, A Study in Atmospheric Optics. Plenum Press, New York, 1966, 358p.

24. Weather Underground, 2008. http://www.weatherunderground.com/history/airport/KBCT/2008/2/19/MonthlyHistory.html

25. Kreith, K., and Kreider, J.F., Principles of Solar Engineering. Hemisphere,Washington DC, 1978, 778p.

26. Green, W.E., "Correcting for atmospheric extinction", *Int. Comet Quarterly*, **14**, 1992, 55-59.

27. Morran, J.M., and Shapiro, H.N., Fundamentals of Engineering Thermodynamics. John Wiley, New York, 1988, 803p.

28. GOES Aerosol/Smoke Product, 2008. http://www.ssd.noaa.gov/PS/FIRE/GASP/gasp.html

29. NCDC, National Climate Center, NOAA, United States Department of Commerce, 2008. http://lwf.ncdc.noaa.gov/oa/ncdc.html